Available online at www.sciencedirect.com

ScienceDirect

Procedia Structural Integrity 75 (2025) 10–18

Structural Integrity Procedia

www.elsevier.com/locate/procedia

Fatigue Design 2025 (FatDes 2025)

Significant improvement of the fatigue performance of ER70S-6 WAAM un-milled structures: A Cu/Ni multilayer nanotechnology approach

Mohsen Falah[a]*, Robert Lau[b], Niclas Spalek[a], Maren Seidelmann[a], Nikolay Lalkovski[a], Marcus Rutner[a]

[a]*Hamburg Institute of Technology, Denickestraße 17, 21073 Hamburg, Germany*
[b] *Fraunhofer-Einrichtung für Additive Produktionstechnologien IAPT, Am Schleusengraben 14, 21029 Hamburg, Germany*

Abstract

In recent years, the adoption of Wire Arc Additive Manufacturing (WAAM), now defined as Directed Energy Deposition based on Gas Metal Arc Welding (DED-Arc), in steel construction has increased significantly. However, the sequential layer deposition inevitably creates surface notches that cause high stress concentrations, leading to fatigue crack initiation. The current industrial standard for post-processing, CNC milling, is time-consuming and resource-intensive. A novel research approach focuses on directly controlling critical residual stresses of as-built specimens by introducing near-surface compressive residual stresses using a Cu/Ni nanostructured metallic multilayer (NMM). This study investigates the effect of NMM on DED-Arc structures and extends its application to metallic 3D-printed components. Optical microscopy provides detailed surface morphology and reliable roughness measurements, while X-ray diffraction (XRD) confirms the presence of residual tensile stresses in the NMM and the resulting residual compressive stresses in the steel substrate. Preliminary tension-tension fatigue testing provides insights into the fatigue strength increase due to NMM treatment of DED-Arc dogbone specimen.

Peer-review under the responsibility of Dr Fabien Lefebvre with at least 2 reviewers per paper

Keywords: Nanometallic Multilayer; Post-Print Treatment; Directed Energy Deposition based on Gas Metal Arc Welding (DED-Arc); Fatigue Resistance; Lifetime Extension

1. Introduction

Fatigue fractures are responsible for approximately 80% of all structural failures, representing a significant concern within the field of civil engineering (Das, 1997). In recent years, the incorporation of 3D printing into steel

Peer-review under the responsibility of Dr Fabien Lefebvre with at least 2 reviewers per paper
10.1016/j.prostr.2025.11.002

construction practices has gained considerable traction. The cross section is developed in successive layers, facilitated by a collaborative robotic arm. Surface notches associated with the welding process are unavoidably generated when the layers are deposited sequentially. These surface notches exhibit substantial stress concentrations, which act as the origins for fatigue crack initiation under conditions of dynamic loading (Bartsch et al., 2021; Das, 1997). A potential approach to avoid these notches involves the laborious and energy-demanding process of mechanical surface milling (Chernovol et al., 2021).

An innovative method focuses on the direct management of critical residual stresses by introducing residual compressive stresses at the surface level by utilizing a micrometer-sized Cu/Ni nanostructured metallic multilayer (NMM) (Brunow and Rutner, 2021, Brunow et al. 2023). The outcomes correspond with earlier studies that analyzed the mechanical properties of Cu/Ni nanolaminate coatings (McDonald et al., 2019). The multilayer is processed via electroplating technology in a controlled laboratory environment. The individual layer thicknesses of the electroplated copper and nickel layers are controlled by the current density (Kanani, 2020).

This research initiative is driven by the objective of creating an effective post-print treatment designed to enhance the usable lifespan of cyclically loaded 3D-printed structures using Directed Energy Deposition based on Gas Metal Arc Welding (DED-Arc). Findings from tension-tension fatigue tests of steel dogbone specimen with a central double-sided V-butt weld indicate a significant improvement in the fatigue strength when the welds are treated by NMM (Brunow et al., 2022; Brunow et al., 2023). The results show a very reduced scatter in the S-N-diagram underscoring the high reliability of the method. One of the governing material mechanisms responsible for the significant gain in lifetime and increase of fatigue strength are residual stresses. The tensile stresses caused within the nanolaminate during processing of the NMM produce advantageous compressive stresses in the steel substrate, which postpone or even prevent crack initiation (Brunow et al., 2023). Rutner et al. (2024, 2025) emphasize the potential of using NMM in structural engineering, hence, applying the superior nanomaterial properties for compensating weaknesses in macro design and eventually improving the long-term structural integrity of steel infrastructure. Please note that the NMM thin film applied on the steel structural member does not contribute in carrying any internal forces such as strengthening millimeter-sized laminates, e.g. Fiber Metal Laminates (Woelke et al., 2015), which have the disadvantage of having a significant stiffness change along the edges, hence, creating a new notch. In contrast, the NMM because of the micrometer-sized thickness does not lead to stiffness discontinuities at the edge but induces compressive stresses at and adjacent to the steel surface suppressing dents and microcracks. The NMM post-weld-treatment has been developed over the last years from small-scale laboratory tests (Brunow et al., 2021; Brunow and Rutner, 2021; Ramezani et al., 2017) to a scalable technology (Brunow et al., 2022) by using electrodeposition, applicable for new and existing structures (Rutner et al., 2024, 2025; Seidelmann et al., 2025).

2. Experimental Setup

2.1 Specimen Preparation

A thin-walled rectangular structure is fabricated by Fraunhofer IAPT using DED-Arc, shown in Fig. 1(a). The nominal wall thickness is 2.5 mm . The DED-Arc system setup consists of a KUKA KR60HA robot and a Fronius TPSi400 welding source. The welding electrode material is ER70S-6 (EN ISO 14341-A G 46 4 M21 4Si1) steel wire with a diameter of 1.2 mm. The chemical composition and mechanical properties of the feedstock wire, as reported by the manufacturer, are listed in Tables 1 and 2, respectively. The DED-Arc geometry is fabricated on a 200 x 200 x 10 mm³ S355J0 steel base. A continuous robot path without waiting times was used as path planning strategy. Fig. 1(a) shows a defect on the upper section of the rear short wall of the rectangular prism. This side of the specimen is not used for samples.

A summary of the key DED-Arc process parameters, as provided by the manufacturer, is provided in Table 3. A parameter set with low energy input is selected to be able to print the thin-walled geoemtry. Therfore, the welding variant Cold Metal Transfer (CMT), more precisly the mode cycle step, is used. Samples for static and fatigue testing are cut out from the DED-Arc plates through Wire EDM, with the longitudinal axis of each sample positioned orthogonally to the deposition direction. The specimen geometry is chosen according to Type E, DIN 50125 (2022), see Fig. 1(b) and (c). The roughness of the DED-Arc samples is evaluated to understand how surface roughness caused by the manufacturing process effects the mechanical and fatigue properties. It is observed that the materials of base

plate and DED-Arc welding material mix which occurs only locally in the transition area between base plate and 3D-printed material. However, the specimen are cut out from locations away from the base plate and have the pure material properties of the feedstock wire.

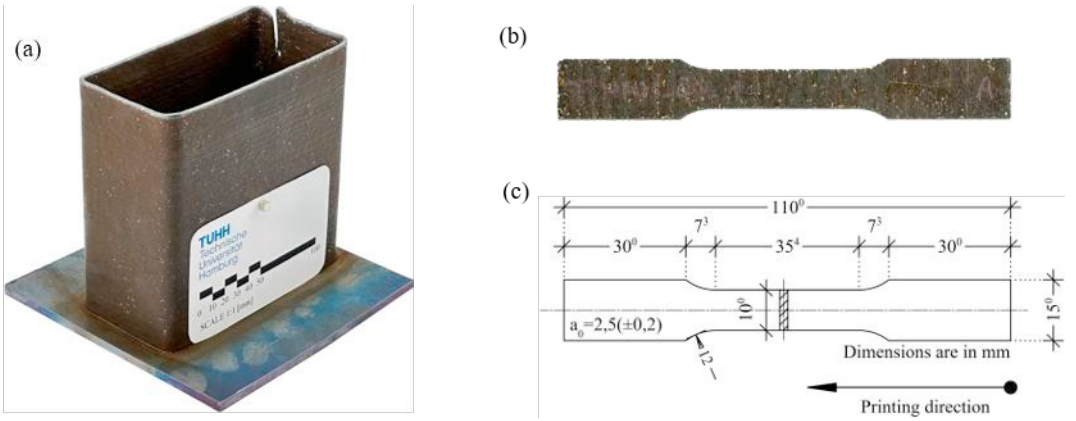

Fig. 1. (a) WAAM rectangular prism of 2.5 mm nominal thickness by Fraunhofer IAPT; (b) Dogbone sample after cutting using Wire EDM; (c) Monotonic and fatigue dogbone specimen geometry according to DIN 50125:2022-08.

Table 1. Chemical composition (in % by weight) of ER70S-6 wire from the manufacturer's datasheet.

Feedstock wire	C	Si	Mn	Fe
ER70S-6 (G 46 4 M21 4Si1)	0.1	1.0	1.7	balance

Table 2. Mechanical properties of ER70S-6 wire from the manufacturer's datasheet.

Feedstock wire	Yield strength [MPa]	Tensile strength [MPa]	Elongation [%]	Impact energy at 40 °C [J]
ER70S-6	480 (≥ 460)	530 – 680	26 (≥ 20)	50 (≥ 47)

Table 3. Process parameters used for DED-Arc plates produced by IAPT Fraunhofer.

Process parameter	Unit	Value
Feedstock wire	[-]	ER70S-6 (G 46 4 M21 4Si1)
Welding mode	[-]	CMT cycle step
Travel speed	[mm/s]	10.0
Wire feed rate	[m/min]	4.0
Shielding gas	[-]	82% Ar + 18% CO2
Gas flow rate	[L/min]	15.0

After the dogbone samples are cut using Wire EDM with a MV1200S (©Mitsubishi Electric Corporation, Japan), they undergo a clean blasting treatment with steel beads S110 to remove the welding soot produced in the manufacturing process. Clean blasting is performed at a pressure of 5.8 bar, at an impact angle of 60 degrees and a distance of 28 cm. In order to prevent stress concentrations, all edges of the dogbone specimen are smoothened prior to testing. No additional mechanical surface treatments are used. The cleaning process before electroplating involves an ultrasonic bath for 10 minutes with a 2,5% solution EM-600 (emmi® EMAG AG, Germany) followed by a 5-minute ultrasonic rust removal using a 5,0% solution of EM-202 (emmi® EMAG AG, Germany). This sequence of treatments ensures that the surfaces are entirely free of rust and grease.

2.2. Characterization of surface profile

The surface roughness is evaluated using the KEYENCE VHX7000 optical microscope equipped with a VH-ZST dual objective (KEYENCE®, Japan) in accordance with recommendations in (Volk, 2018). Measurements are

executed along five distinct lines on both sides, maintaining a distance of 1.0 mm between each line. This procedure allows a more accurate determination of the existing surface roughness. The average value is derived from a set of 80 and 30 data points for the as-build state and after combined clean blasting and NMM, respectively. The geometric characteristics of the constructed static and fatigue specimen, encompassing the surface roughness parameters, are detailed in Table 5.

2.3. X-ray diffraction

The Xstress DR45 system (Stresstech®, Ireland) utilizes two 2D detectors with a resolution of 256 × 256 pixels (55 µm pixel size), enabling precise and detailed stress measurements. The polynomial regression is chosen according to Savitzky-Golay (Savitzky and Golay, 1964), as this approach preserves the important peak height of the data. The experimental configuration is established to investigate the stress distribution in nickel- and copper-layers, where X-ray diffraction measurements are performed using a modified χ mode. The study focuses on the *Ni {220}* and *Cu {220}* crystallographic planes, with the X-ray tube utilizing *Cr Kα* radiation with a wavelength of approximately 2.289700 Å. Data collection occurs over a range of tilt angles ψ from -45.0° to +45.0°, with each measurement having a designated exposure time of 5 seconds. The diffraction pattern is centered around mid 2θ angles of *127.4°* and *133.7°*, which provides significant insights into the lattice parameters of Cu and Ni, respectively. The detector is calibrated with a threshold of 70% and positioned at a fixed distance of 45 mm from the sample, featuring a pixel size of 55 µm to ensure high spatial resolution.

2.4. Monotonic and Fatigue Tests

Mechanical characteristics related to stress and strain of DED-Arc materials are analyzed through tensile specimen testing, shown in Fig. 1(b), which is carried out at room temperature in accordance with DIN EN ISO 6892-1 (2020). In the tests conducted, the load is applied displacement controlled until failure at strain rates according to DIN EN ISO 6892-1 Method B, with a gradual transition ramp implemented between the two rates.

All monotonic tensile tests are performed under uniaxial loading conditions with the Zwick/Roell Z100 (ZwickRoell GmbH & Co. KG, Germany) in the Structures Laboratory. The fatigue tests are executed under sinusoidal loading conditions with a Schenck Hydropuls PSB servo-hydraulic machine (©Illinois Tool Works Inc, USA).

Force-displacement data obtained from the test are captured electronically. The yield strength f_y is defined at the point of inflection on the force-displacement curve. The ultimate strength f_u is recorded at the apex of the curve. Stress-strain curves are computed using the nominal cross-sectional area A_{nom} and the original gauge length L_0.

The DED-Arc specimens are tested in a tension-tension fatigue setting with a stress ratio $R = 0.1$ and a frequency of 8 Hz. The test assessment is conducted using linear regression with the following formula (Schneider and Maddox, 2003):

$$\log N = \log(A) - m * \log(S) \tag{1}$$

where N is the endured number of cycles on the nominal stress range level S, A is the reference fatigue strength at $2x10^6$ cycles, and m the free inverse slope.

2.5. Multilayer Electroplating

In the process of electroplating, the samples are coated using a galvanostatic pulse plating power supply (Plating Electronics®, Germany) and a sulphate-based electrolyte according to Bonhôte and Landolt (1997). Utilizing the single-bath immersion galvanization method, layers of nickel and copper are deposited alternately resulting in individual layer thicknesses of 35 nm and 5 nm, respectively. A 1,000 nm nickel-levelling-layer is applied on the DED-Arc-substrate, since it indicates to smoothen out sub micro surface irregularities.

The control of the layup is determined by the interplay of current density and time, in accordance with Faraday's

Law (Faraday, 1834) and the principles outlined in the Cottrell equation (Cottrell, 1903). Employing these two principles enables the manipulation and specification of layer thickness by varying both, the current density and the time interval during which the current is applied. Table 4 outlines the essential parameters associated with the electroplating process. For the purpose of ensuring a uniform current density on the anode surface, these are set up in parallel and connected to the pulse plating power supply, as shown in Fig. 2(b).

Sodium citrate serves as a complexing agent in the process of electrochemical coating, primarily functioning to stabilize metal ions within the solution and enhance their electrolysis potential.

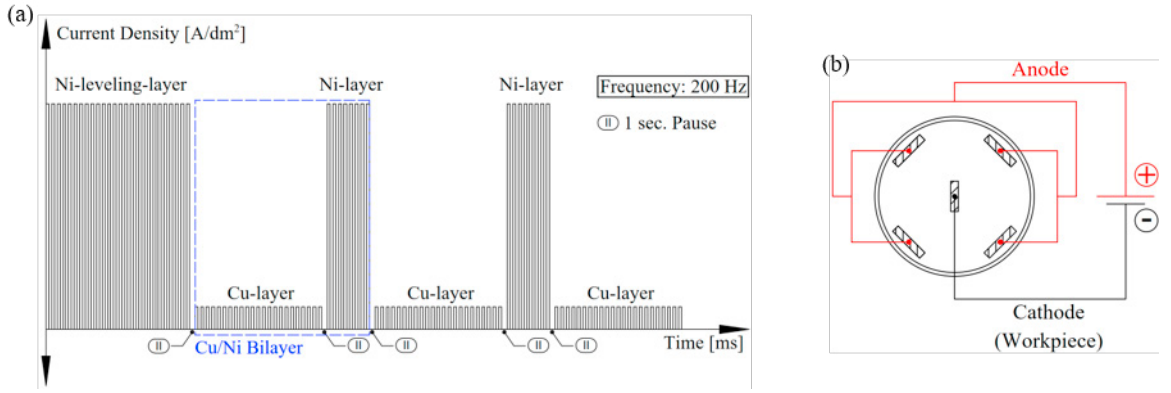

Fig. 2. (a) Schematic representation of the current-controlled squared unipolar duplex pulse waveform for Cu/Ni multilayer electroplating; (b) Electrical circuit showing the parallel setup of anodes in the electroplating cell.

Table 4. Electroplating parameters of the current-controlled duplex pulse of Cu/Ni multilayer.

Parameter	Unit	Ni-levelling-layer	Ni-layer	Cu-Layer
On-time (T_{on})	[s]	39.0	6.4	31.0
Off-time (T_{off})	[s]	156.0	1.6	124.0
Pulse frequency	[Hz]	200	200	200
Duty cycle:	[-]	20	20	20
Peak current density	[A/dm²]	11.0	11.0	0.225
Avg. current density	[A/dm²]	2.20	2.20	0.045
Deposition time	[s]	195.0	8.0	155.0
Ph-Value	[-]	4.5	4.5	4.5
Stirring speed	[rpm]	850	850	850
Bath temperature	[°C]	20.0	20.0	20.0

3. Results

3.1. Surface Roughness

In this part, the outcomes of the roughness assessment are examined. Clean blasting of the DED-Arc samples leads to a change in the surface morphology and in residual compressive stress-built-up of the DED-Arc samples. DED-Arc-specimen produced by CMT technology cause an average mean arithmetic roughness of 77 µm. The NMM deposited on top of the clean-blasted DED-Arc surface shows an average mean arithmetic roughness of about 66 µm. Observations made under an optical microscope indicate a non-uniform surface of the as-built DED-Arc section, resulting from the solidification of the weld pool, as shown in Fig. 3(a). After undergoing clean blasting, the lunar crater topography displays a more uniform surface texture with circular crater boundaries, as shown in Fig. 3(b). Fig. 3(c) presents an image depicting the surface morphology of the electrodeposited metallic Cu/Ni multilayer deposited on the clean-blasted specimen.

Table 5. Surface roughness analysis of the DED-Arc samples: a) As-built; b) After clean blasting; c) After clean blasting and NMM application.

Measuring	Data points	R_a [µm]	R_{max} [µm]	R_q [µm]
a) As-built	80	77	383	95
b) Clean blasting	30	61	294	74
c) Clean blasting + NMM	30	66	317	81

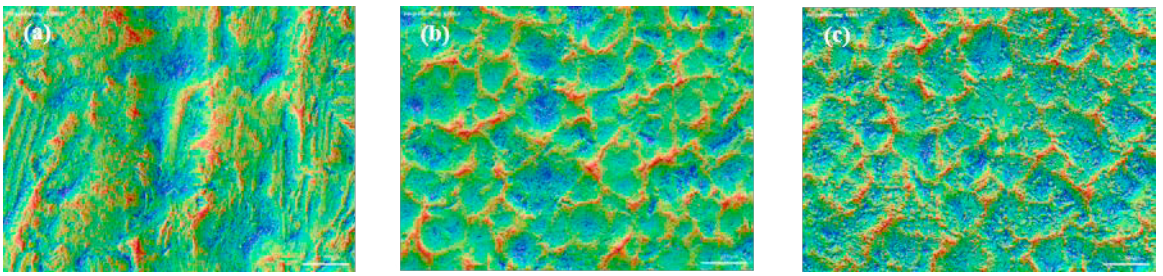

Fig. 3. Optical microscope analysis of the surface morphology under the microscope at 200x magnification of (a) as-built; (b) after clean blasting; (c) after clean blasting and NMM electroplating.

3.2. Residual stresses

As shown in Figure 4(a), detector A captures a standard left shift of the peak at the Fe {211}, which serves as an indicator of residual compressive stresses. Conversely, detector B exhibits a mirrored response (right peak shift), which similarly suggests the presence of compressive stresses. The measurements are recorded after clean blasting confirming significant and uniformly distributed residual compressive stress inserted into the sample surface (Totten et al., 2002). The measured residual compressive stresses are about -270 MPa. Due to the limited penetration depth of the radiation produced by the laboratory *Cr* X-ray tube, stress measurements of the NMM-treated samples only provide residual stress measurement of the nanometal multilayer, however not for the steel substrate. Residual tensile stress in the order of +790 MPa is measured for the nickel layer and +390 MPa for the copper layer. Measurements are performed on *Ni {220}* at 2θ=133.7° and on *Cu {220}* at 2θ=127.4°, respectively. Hence, without having measured residual compressive stresses in the steel substrate of the nanolaminated DED-Arc sample, however, noticing the agreement with measurements by Spalek et al. (2025), desired residual compressive stresses at the DED-Arc sample surface and adjacent to the surface can be expected. The findings of the XRD analysis are detailed in Table 6.

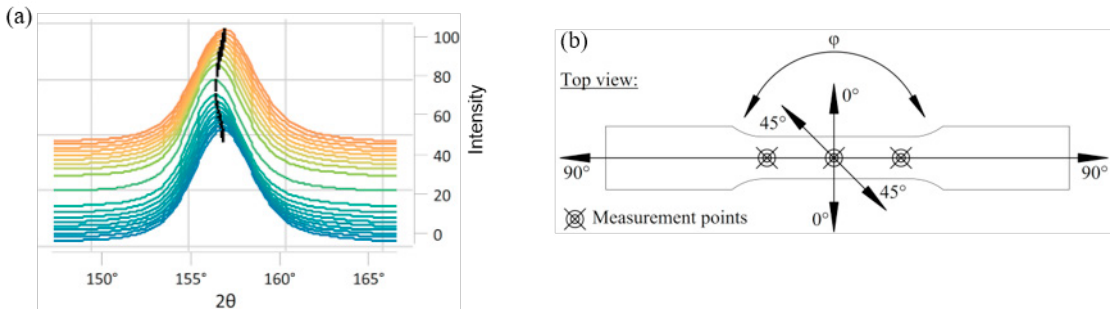

Fig 4. (a) Fe {211} peak shift at 2θ = 156.8° after clean blasting, with various ψ from -45° to +45°; (b) In plane Rotation angles.

Table 6. Avg. residual stresses in MPa at the rotation angles 0°, 45°, 90°; (-) compression and (+) tension.

Rotation angle	As-built	Clean blasting	Clean blasting + NMM	
	Fe {211}	Fe {211}	Ni {220}	Cu {220}
	$2\theta = 156.8°$	$2\theta = 156.8°$	$2\theta = 133.7°$	$2\theta = 127.4°$
0°	+64.1	-282.4	+789.6	+397.4
45°	+70.4	-285.6	+799.5	+400.2
90°	+68.0	-270.9	+808.3	+406.8

3.3. Monotonic Tensile Test

The engineering stress-strain curves and the material properties are discussed in this section. The essential material properties are extracted from the acquired stress-strain curves, which are Young's modulus E, yield strength f_y, ultimate tensile strength f_u, strain at ultimate tensile strength ε_u, and the fracture strain across the specified gauge length ε_f. The as-built specimen shows a slightly angled yield plateau, which is explained by the multi-undulating surface. The yield strength is defined as the 0.2% proof stress. The ductility of the as-built specimen meets the Eurocode 3 requirements pertaining to hot-rolled steels. Table 7 provides an overview of the material properties.

It is further noted that remelting of the material during the DED-Arc process results in the deposited material having a lower strength compared to the values stated by the manufacturer for conventional welds, which is consistent with findings in the literature (Huang et al., 2022).

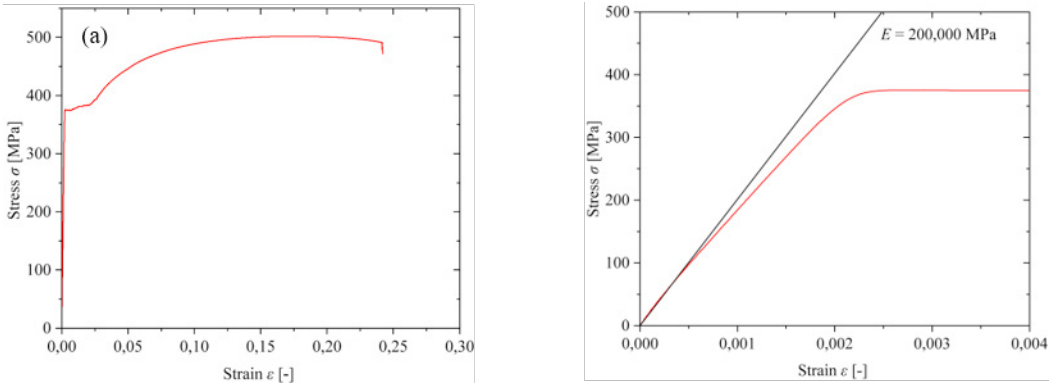

Fig 5. Stress-strain curves of the as-built WAAM specimen: (a) full strain range; (b) enlarged elastic-plastic transition.

Table 7. Effective material properties of as-built coupon with a nominal thickness of 2.5 mm.

ID	E [MPa]	f_y [MPa]	f_u [MPa]	ε_f [-]	ε_u [-]	$\varepsilon_u/\varepsilon_y$	f_u/f_y
T_AB_90_1	188,000	375	500	0.24	0.17	85	1.33

3.4. Fatigue Test – S/N curve

In this section, a fatigue assessment of the DED-Arc material is conducted based on nominal stresses. The nominal stress ranges $\Delta\sigma_{nom}$ for the tested as-built specimen are plotted in log-log scale against the number of cycles to failure N_f, as shown in Fig. 6. An inverse slope exponent of m = 3.0 is defined, as suggested in EN 1993-1-9 ("DIN EN 1993-1-9," 2010) and in the IIW Recommendations (Hobbacher and Baumgartner, 2024). The fitted S-N curve is shown in Fig. 6 along with a survival probability $\Delta\sigma_{R,50\%} = 50\%$ determined by assuming a log-normal distribution of fatigue life N_f for the evaluated stress level. The analysis of NMM treated samples demonstrates a significantly improved fatigue resistance.

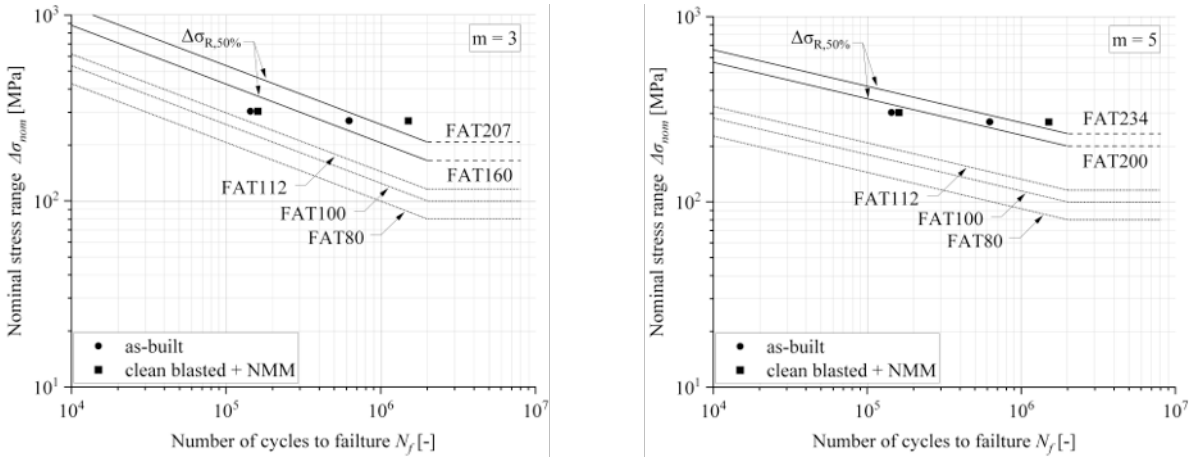

Fig 6. Fitted S-N diagram based on nominal stress readings from fatigue test results.

Table 8. Fatigue test (F) results for as-built (AB) and NMM coated (NMM) samples.

Sample ID	R	$\Delta\sigma_{nom}$ [MPa]	σ_{max} [MPa]	σ_{min} [MPa]	Reason for termination	N_f [-]
F_AB_90_1	0.1	303.8	337.5	33.8	Fracture	143,704
F_AB_90_2	0.1	270.0	300.0	30.0	Fracture	623,347
F_NMM_90_1	0.1	303.8	337.5	33.8	Fracture	160,321
F_NMM_90_2	0,1	270.0	300.0	30.0	Fracture	1,506,400

4. Conclusion

This study primarily investigates the fatigue behaviour of DED-Arc plates built from ER70S-6 (G 46 4 M21 4Si1) steel wire produced via CMT technology. The DED-Arc specimen subsequently underwent clean blasting using S110 steel spheres with 5.8 bar and nanometal multilayer (NMM) post-print treatment. Monotonic tension tests revealed that the Young's modulus of the DED-Arc specimens is similar to that of conventional steels, demonstrating satisfactory ductility and load-bearing capacity. However, the DED-Arc process resulted in a 20%-reduction in strength of the deposited material when compared to the values provided by the manufacturer for traditional welds.

Clean blasting of the DED-Arc samples led to a change in the surface morphology and in residual compressive stress-built-up of the DED-Arc samples. DED-Arc-specimen produced by CMT technology caused an average mean arithmetic roughness of 77 µm. The NMM deposited on top of the clean-blasted DED-Arc surface showed an average mean arithmetic roughness of about 66 µm. While the as-built samples showed residual tensile stresses of +70 MPa, clean blasting consistently converts these residual tensile stresses into near-surface residual compressive stresses of about - 270 MPa. XRD assessment of clean-blasted and NMM-treated DED-Arc specimen revealed the presence of residual tensile stresses in the NMM in the order of about +790 MPa and +390 MPa in Ni and Cu individual nanolayers, respectively. The XRD applied herein was able to measure stresses up to a depth of about 3.0 µm from the NMM surface. Hence, measuring the compensating compressive residual stresses in the DED-Arc substrate and their distribution across the thickness requires a more powerful XRD source. These measurements are planned in the near future.

Tension-tension fatigue tests with dog-bone shaped DED-Arc samples has been conducted with a stress ratio of R=0.1. Two as-built samples were tested for fatigue at maximum stress amplitudes of 80% and 90% of the yield strength, which resulted in notably different fatigue cycle numbers of 620,000 and 140,000 cycles, respectively. The clean-blasted and NMM-treated DED-Arc samples tested at 80% and 90% of the yield strength achieved cycle numbers of 1,506,400 and 160,321 cycles, which is a first indicator of the achievable increased fatigue strength through the combined clean blasting and NMM-treatment. The initial findings reported in this report are promising,

providing fundamental insights into the combined effects of clean-blasting and NMM-treatment on DED-Arc structural members. Further measurements must be performed with additional samples to obtain statistically reliable results and a first S-N-curve of NMM-treated DED-Arc samples and to quantify the fatigue strength increase contributed by clean blasting and NMM-treatment, respectively.

5. Acknowledgements

The authors acknowledge Fraunhofer IAPT for producing the DED-Arc specimen.

References

Bartsch, H., Kühne, R., Citarelli, S., Schaffrath, S., Feldmann, M., 2021. Fatigue analysis of wire arc additive manufactured (3D printed) components with unmilled surface. Structures 31, 576–589. https://doi.org/10.1016/j.istruc.2021.01.068

Bonhôte, Ch., Landolt, D., 1997. Microstructure of Ni-Cu multilayers electrodeposited from a citrate electrolyte. Electrochimica Acta 42, 2407–2417. https://doi.org/10.1016/S0013-4686(97)82474-7

Brunow, J., Gries, S., Krekeler, T., Rutner, M., 2022. Material mechanisms of Cu/Ni nanolaminate coatings resulting in lifetime extensions of welded joints. Scr. Mater. 212, 114501. https://doi.org/10.1016/j.scriptamat.2022.114501

Brunow, J., Ritter, M., Krekeler, T., Ramezani, M., Rutner, M., 2021. Thermal stability of a nanolayered metal joint. Scr. Mater. 194, 113687. https://doi.org/10.1016/j.scriptamat.2020.113687

Brunow, J., Rutner, M., 2021. Das Nanolaminatpflaster – Schweißnahtnachbehandlung für bisher unerreichte Lebensdauerverlängerung. Stahlbau 90, 691–700. https://doi.org/10.1002/stab.202100042

Brunow, J., Spalek, N., Mohammadi, F., Rutner, M., 2023. A novel post-weld treatment using nanostructured metallic multilayer for superior fatigue strength. Sci. Rep. 13, 22215. https://doi.org/10.1038/s41598-023-49192-0

Chernovol, N., Sharma, A., Tjahjowidodo, T., Lauwers, B., Van Rymenant, P., 2021. Machinability of wire and arc additive manufactured components. CIRP J. Manuf. Sci. Technol. 35, 379–389. https://doi.org/10.1016/j.cirpj.2021.06.022

Cottrell, F.G., 1903. Der Reststrom bei galvanischer Polarisation, betrachtet als ein Diffusionsproblem. Z. Für Phys. Chem. 42U, 385–431. https://doi.org/10.1515/zpch-1903-4229

Das, A.K., 1997. Metallurgy of failure analysis. McGraw-Hill, New York.

DIN 50125:2022-08, Prüfung metallischer Werkstoffe_- Zugproben, 2022. https://doi.org/10.31030/3337825

DIN EN 1993-1-9:2010-12, Eurocode_3: Bemessung und Konstruktion von Stahlbauten_- Teil_1-9: Ermüdung; Deutsche Fassung EN_1993-1-9:2005_+ AC:2009, 2010. https://doi.org/10.31030/1722660

DIN EN ISO 6892-1:2020-06, Metallische Werkstoffe_- Zugversuch_- Teil_1: Prüfverfahren bei Raumtemperatur (ISO_6892-1:2019); Deutsche Fassung EN_ISO_6892-1:2019, 2020. https://doi.org/10.31030/3132591

Faraday, M., 1834. VI. Experimental researches in electricity.-Seventh Series. Philos. Trans. R. Soc. Lond. 124, 77–122. https://doi.org/10.1098/rstl.1834.0008

Hobbacher, A.F., Baumgartner, J., 2024. Recommendations for Fatigue Design of Welded Joints and Components, IIW Collection. Springer Nature Switzerland, Cham. https://doi.org/10.1007/978-3-031-57667-6

Huang, C., Kyvelou, P., Zhang, R., Ben Britton, T., Gardner, L., 2022. Mechanical testing and microstructural analysis of wire arc additively manufactured steels. Mater. Des. 216, 110544. https://doi.org/10.1016/j.matdes.2022.110544

Kanani, N., 2020. Galvanotechnik: Grundlagen, Verfahren und Praxis einer Schlüsseltechnologie, 3., aktualisierte Auflage. ed. Hanser, München.

McDonald, I.G., Moehlenkamp, W.M., Arola, D., Wang, J., 2019. Residual Stresses in Cu/Ni Multilayer Thin Films Measured Using the Sin2ψ Method. Exp. Mech. 59, 111–120. https://doi.org/10.1007/s11340-018-00447-2

Ramezani, M.G., Demkowicz, M.J., Feng, G., Rutner, M.P., 2017. Joining of physical vapor-deposited metal nano-layered composites. Scr. Mater. 139, 114–118. https://doi.org/10.1016/j.scriptamat.2017.06.032

Rutner, M., Lalkovski, N., Falah, M., Seidelmann, M., Spalek, N., 2025. Merging nano and macro structure design: Opportunities for the structural integrity of steel infrastructure. Struct. Integr. Procedia.

Rutner, M., Spalek, N., Falah, M., Lalkovski, N., 2024. Verknüpfung von Nano mit Makro – Chancen für den Stahlbau. Stahlbau 93, 584–596. https://doi.org/10.1002/stab.202400048

Savitzky, Abraham., Golay, M.J.E., 1964. Smoothing and Differentiation of Data by Simplified Least Squares Procedures. Anal. Chem. 36, 1627–1639. https://doi.org/10.1021/ac60214a047

Seidelmann, M., Spalek, N., Falah, M., Lalkovski, N., Rutner, M., 2025. Enhancing the Lifespan of Steel Structures through a 3D-printed Coating Device for the Application of a Nanometallic Multilayer on Weld Seams. Struct. Integr. Procedia.

Spalek, N., Falah, M., Seidelmann, M., Lalkovski, N., Abreu Faria, G., Rutner, M., 2025. Material mechanisms of the nanostructured metallic multilayer post-weld treatment for fatigue strength increase. Struct. Integr. Procedia.

Totten, G.E., Howes, M.A.H., Inoue, T. (Eds.), 2002. Handbook of residual stress and deformation of steel. ASM International, Materials Park, Ohio.

Woelke, P.B., Rutner, M.P., Shields, M.D., Rans, C., Alderliesten, R., 2015. Finite Element Modeling of Fatigue in Fiber–Metal Laminates. AIAA J. 53, 2228–2236. https://doi.org/10.2514/1.J053600